Journal of Building Engineering 89 (2024) 109323

Contents lists available at ScienceDirect

Journal of Building Engineering

journal homepage: www.elsevier.com/locate/jobe

Experimental and numerical investigation of a real-scale air to multiple PCM heat exchanger

Bashir Eskander Kareem *, Ahmed Mohammed Adham, Banipal Nanno Yaqob

Department of Technical Mechanical and Energy Engineering, Erbil Technical Engineering College, Erbil Polytechnic University, Erbil, Iraq

ARTICLE INFO

Keywords:
Phase change materials
Multiple PCM-To-air heat exchanger
Latent heat storage system
Free cooling

ABSTRACT

Energy consumption by residential sectors has proliferated due to urbanization and lifestyle changes. Passive cooling and heating systems can reduce energy consumption and CO_2 emissions in residential and commercial sectors. Phase change materials provide an efficient solution for passive energy storage, addressing a building's needs for free cooling and heating. These materials absorb and release heat energy, enhancing the overall efficiency of the energy management system. By employing energy storage devices, it becomes feasible to reduce and shift peak loads to off-peak hours. This study optimized the size and configuration of air-to-multiple PCM heat exchanger through the utilization of a 2D ANSYS (Fluent 19.2) model. This study employs multiple phase change materials (PCMs) with varying melting temperatures as a heat transfer technique to reduce the melting and solidifying times of the PCMs. Furthermore, it was observed that the arrangement of PCMs in series affected melting and solidification times, so two scenarios have been examined. The air-to-multiple PCM system has been investigated through numerical simulations and experimental analyses, focusing on the liquid fractions within the PCM and the outlet air temperatures across the air channels. The total time for entirely melting PCMs RT25HC and RT21HC is less than 4 h, but the solidification time for PCM-RT21HC needs more than 12 h. In both scenarios, PCM-RT21HC melted first, while PCM-RT25HC solidified first.

Nomenclature

H	Height (m)
L	Length (m)
T	Temperature (°C)
W	Width (m)

Abbreviations

CFD	Computational fluid dynamics
HTF	Heat transfer fluid
HVAC	Heating, ventilation and air conditioning
IEA	International Energy Agency
PAHX	PCM to air heat exchanger

* Corresponding author.
E-mail address: bashir.kareem@epu.edu.iq (B.E. Kareem).

https://doi.org/10.1016/j.jobe.2024.109323
Received 2 February 2024; Received in revised form 6 April 2024; Accepted 13 April 2024
Available online 16 April 2024

PCM	Phase change material
SSPCM	Shape-stabilized phase change material
TES	Thermal energy storage

1. Introduction

Global power consumption has climbed around 18 % in the last 10 years, which will expand to 30 % in 2040 [1]. Buildings consume 40 % of total energy, as stated in a report from the International Energy Agency (IEA), and this sector has experienced rises in electricity and natural gas use of 11.1 % and 9.4 %, respectively [1]. Passive technologies and energy-efficient solutions will improve indoor thermal comfort while using minimal energy, thus deterring the global warming crisis. Passive technologies make it feasible to reduce peak load [2]. A building's free cooling system uses natural temperature fluctuations to cool indoor air, with absorbing and releasing energy in PCMs. This approach minimizes dependence on air conditioning systems and concurrently enhances their overall efficiency [3]. PCMs have been applied in residential buildings to address surface temperature concerns and reduce carbon dioxide emissions. The study examines various scenarios, including the utilization of PCM on roofs and its integration with solar panels. The results reveal a significant maximum annual cooling load reduction of 14,521.6 kWh, accompanied by 22.55 % reduction in overall loads on PV panels. This system emerges as the optimal choice for both cost and energy savings, supported by its estimated seven-year payback period [4]. Implementing PCMs to enhance the efficiency of various systems in Algeria has yielded positive results. The findings demonstrate energy savings of 12 % in refrigeration systems, 17.82 % in air conditioning systems, 10 % in photovoltaics, and a substantial 34.8 % in building envelopes [5]. PCM is employed in conjunction with a heat pump in the ceiling panels for both cooling and heating purposes in a building located in Atlanta. The findings indicate that implementing the suggested strategy can lead to a 27.1 % reduction in electrical costs through the incorporation of PCM into the system [6]. PCMs have been employed in buildings to achieve energy savings and reduce CO_2 emissions. The utilization of PCM in ventilation systems was studied across 15 climates and 45 cities. The primary findings indicate that latent heat storage in a 24-h cycle contributes significantly to energy savings across all climates. Integrating PCM with a controlled ventilation system is deemed practical, sustainable, cost-effective, energy-efficient, and environmentally friendly [7]. Shape-stabilized phase change material (SSPCM) has been integrated into the ventilation system to improve indoor air quality and reduce energy consumption. The results show that incorporating a 30 mm PCM in the roof ventilation system leads to a 2.9 ˚C reduction in peak indoor air temperature, a 5.5 ˚C decrease in peak internal surface temperature, and a 19.2 % reduction in cooling load [8]. PCM is utilized in a wall-type heat recovery and ventilation system to improve thermal energy storage in buildings. The 3D model is employed to optimize configurations and operational variables, resulting in a notable 28.4 % increase in storage rate while simultaneously minimizing costs and pressure drop. Numerical results indicate an enhancement in the system's efficiency from 37.5 % to 44.4 %, contributing to lower energy consumption and the maintenance of indoor air quality [9]. Shell and tube heat exchangers have been widely employed in HVAC systems, contributing to their enhanced performance [10,11]. The application of spiral metal fins in PCM has been implemented to improve natural convection heat transfer. An experimental assessment was carried out on a three-vertical shell-and-tube latent heat storage system to assess the efficiency of annular and spiral fins in comparison to a configuration without fins. The results suggest that the greatest enhancement in heat transfer is achieved when using spiral metal fins. Furthermore, it was observed that annular fins reduce the natural convection effect in PCMs [12]. Multiple PCMs have been incorporated into building design using EnergyPlus to create passive latent heat storage, aiming at energy savings and greenhouse gas reduction. Three PCM layers were added to walls and ceilings. The findings suggest that utilizing multiple PCMs with different melting temperatures is advisable for all climates. The highest annual total load savings, at 11.7 %, were observed in cold climates, while the lowest, at 2.3 %, were in hot climates [13]. The investigation focused on studying the morphologies, chemical compositions, and thermal stability of microencapsulated PCM (MicroPCMs) within building materials, considering different shell-to-core ratios. The board containing 30 % MicroPCM exhibited a substantial 67.82 % increase in thermal mass compared to traditional building materials. Additionally, the results indicated a noteworthy 59 % reduction in indoor temperature fluctuations, demonstrating excellent thermal regulation and the potential for energy savings in buildings [14]. Highly thermally conductive nanoparticles have been widely employed to improve heat transfer in PCMs [15–18]. The experimental study of enhancing the thermophysical properties of paraffin wax has been conducted by employing silver nanoparticles and utilizing nanofluids in solar systems. The addition of nanoparticles at rates of 1 % and 2 % has resulted in an increase in the thermal conductivity of the PCM (paraffin wax) by 35.71 % and 78.57 %, respectively [19]. In an PCM-to-Air Heat Exchanger (PAHX), the PCM panels were exposed to ambient air, causing the air to heat as the PCM solidified and cool as it melted. The PAHX's performance can be enhanced by improving the heat exchanger design more than by improving PCM's thermal properties [20]. In PCMs, conduction heat transfer primarily occurs when the material is in the solid state. Nevertheless, when the panel height exceeds 5 cm, free convection also plays a role in influencing heat transfer rates when the material is in the liquid state [21]. The performance of the PAHX will dramatically drop when the length of the PAHX is greater than 2 m, airflow rates are above 2000 m^3/h, and air channels are less than 1 cm [22]. The present study aims to design and construct flat plate PAHX using multiple PCMs as a heat transfer enhancement (see Table 1). The primary innovation of the current study lies in optimizing the arrangement of PCM layers in PAHX during the melting and solidification processes.

2. Methodology

A 2D model was created utilizing the commercial version of ANSYS Fluent (19.2) to investigate heat and mass transfer in the PAHX between air and multiple PCM. The methodology of the CFD model has been described in earlier research [23]. In this study, a

Table 1
Boundary conditions of the PAHX.

Inlet air temperature	Melting	30 °C
	Solidification	19 °C
The initial temperature of the system	Melting	19 °C
	Solidification	30 °C
Mass flow rate of air	Melting	0.4 kg/s
	Solidification	0.4 kg/s
The flow regime in air channels	Turbulent flow	k-epsilon
The total mass of the PCM	RT21HC	15 kg
	RT25HC	15 kg

PAHX incorporating sixteen PCM panels was employed, where the first eight panels were filled with PCM RT21HC and the subsequent eight panels were filled with PCM RT25HC. As depicted in Fig. (1), air passages surrounded the PCM panels.

In earlier studies, a single PCM was utilized to investigate and numerically optimize the PAHX through the development of a CFD simulation [23]. Prior research has investigated the impact of diverse parameters on the performance of the PAHX. These parameters encompass the dimensions of the PCM panels and air channels, the temperature and flow rate of the inlet air, the length and width of the PAHX, the quantity of PCM panels, the overall mass of PCM, and various PCMs with distinct melting temperatures [23]. The heat rate was elevated, and both the melting and solidification times were reduced through the utilization of multiple PCMs. The optimized dimensions and configuration of the PAHX are detailed in Fig. (1). Prior to the construction of the heat exchanger, optimization was conducted based on the findings from the CFD study. It is crucial to emphasize that the sequence in which PCM layers are arranged in the flow direction directly impacts both the rate of PCM melting and solidification, as well as the effectiveness of the heat exchanger. Table (1) presents the boundary conditions of the model.

The meshing process is the division of CFD fluid domains into a limited number of tiny cells. The mesh quality significantly impacts the accuracy and effectiveness of CFD results. High mesh quality is necessary to generate precise, efficient, and dependable results in Ansys. To reduce computational time, the CFD model was developed in 2D, with negligible changes in the z-direction. The mesh size was determined through a mesh independence test. The fine mesh was used for the system, as shown in Fig. (2). The final mesh with a skewness of 0.35 contains 123,496 elements and 371,317 nodes.

The flow validation is performed for the model by showing the velocity distribution through the PAHX channels, as shown in Fig. (3).

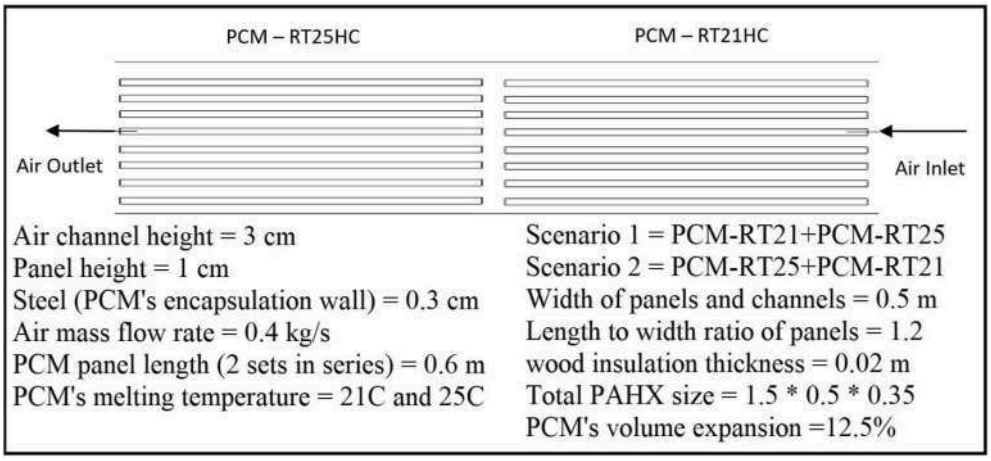

Fig. 1. Schematic of PAHX with optimized dimensions.

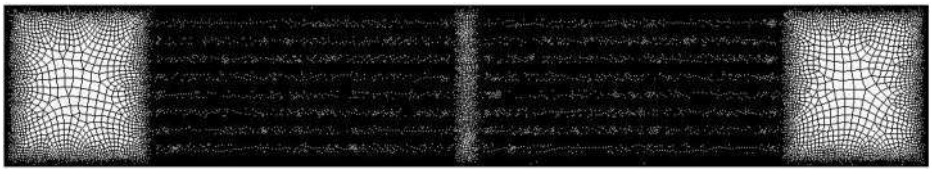

Fig. 2. Fine mesh of the PAHX.

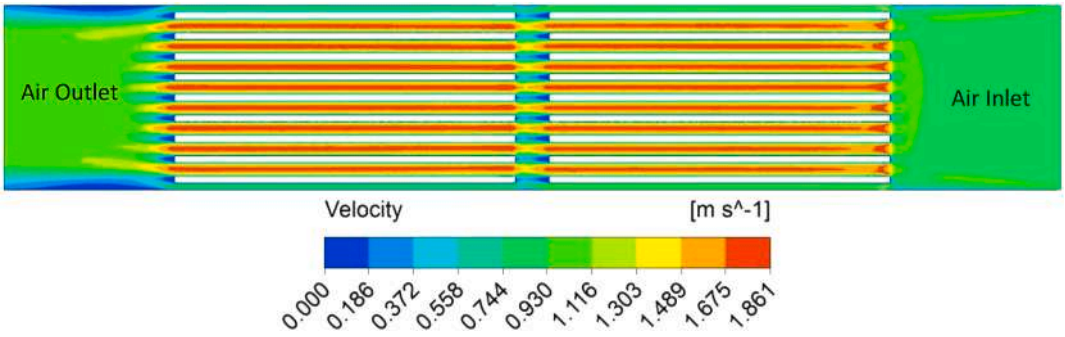

Fig. 3. Velocity contour of the PAHX.

3. Using multiple PCMS in PAHX

The time required for the PCM to undergo melting and solidification stands out as a critical factor influencing the overall effectiveness of the PAHX. Nevertheless, the impact on the durations of melting and solidification can become more intricate when incorporating multiple PCMs with varying melting temperatures in a heat exchanger. In a heat exchanger containing various PCMs with diverse melting temperatures, the PCM with the lowest melting temperature initiates the melting process, followed by the PCM with a higher melting temperature, and so forth. In comparison to employing a single PCM, this sequential melting process might result in an extended total time for both melting and solidification in the heat exchanger. As heat is transferred among PCMs with varying melting temperatures, employing multiple PCMs with distinct melting temperatures can introduce intricate effects on the melting and solidification times within a PAHX. Introducing various PCMs into a PAHX maintains a consistent temperature differential between the PCM and the HTF across the PAHX. Consequently, this enhances the heat transfer rate between the PCMs and HTF. Two scenarios are studied for designing PAHX, the first scenario uses RT21HC in the beginning, and RT25HC will place in the last, as shown in Fig. (4). The second scenario uses RT25HC first, which is followed by RT21HC as shown in Fig. (5). Both scenarios investigated for a thermal cycle through complete melting and solidifying PCM.

4. Experimental work

A flat plate PAHX was employed in an experimental study, and the results were studied. The length, width, and height of the PCM panels are indicated by the symbols *L*, *W*, and *H*, as shown in Fig. (6). The PCM panels and air channels are identical in terms of both length and width. In a previous study, the CFD model was employed to optimize the dimensions of the PAHX and analyze the relevant parameters [23]. The specifications and dimensions of the rig are indicated in Fig. (1). Wood's low thermal conductivity, which inhibits heat gain or loss, led to its selection as the PAHX's insulation material. It was then covered with a layer of 2 cm.

To guarantee an efficient melting and solidification rate in the PAHX, it is crucial to closely monitor the temperature of the HTF in air channels and the proportion of melted PCM in PCM panels. The entire mass of PCMs is 30 kg, evenly distributed between the

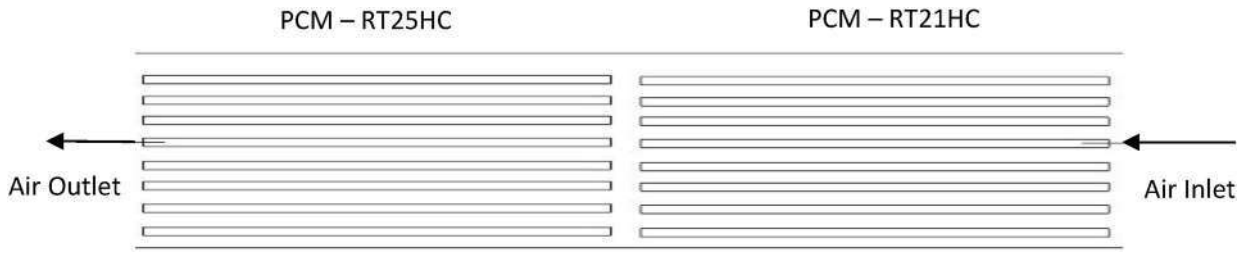

Fig. 4. First scenario of PAHX.

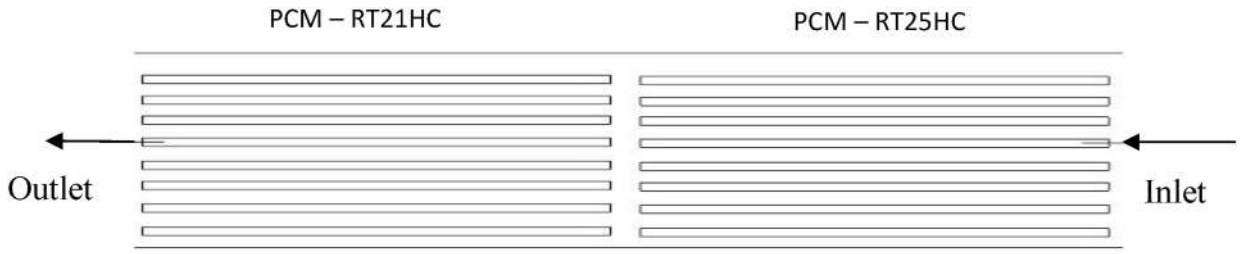

Fig. 5. Second scenario of PAHX.

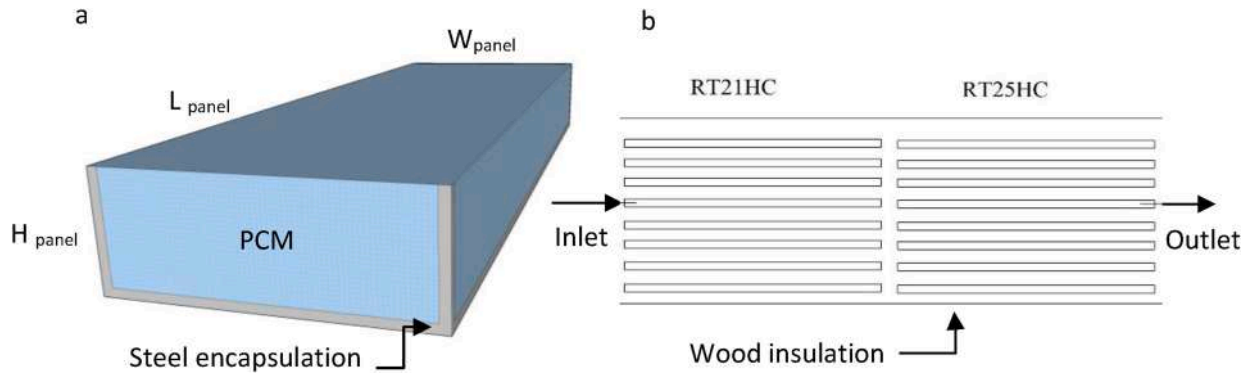

Fig. 6. PAHX dimension (a) a PCM panel and (b) PAHX and air channel [26].

RT21HC and RT25HC types. The experimental investigation of variable airflow rates was carried out using axial fans, a vane anemometer for airflow measurement, type K thermocouples for temperature measurements, and a data logger for recording data. Figures (7 & 8) offer a visual depiction of the experimental setup.

As depicted in Figs. (9 & 10), temperature readings are positioned within the PCM panels and at the inlet and outlet points of the air channels in the PAHX.

The photo of PCMs RT21HC and RT25HC during solidification and melting are shown in Figs. (11 & 12).

Prior to application, the measurements' uncertainties were calculated, and calibration was performed to detect potential errors. The experiment's device uncertainty is presented as an uncertainty error, with temperature and velocity measurements exhibiting uncertainties of approximately ± 0.4 % and ± 4.7 %, respectively.

5. Results and discussions

An experimentally validated CFD model 2D was built and developed by ANSYS (Fluent 19.2). Throughout both the melting and solidifying processes, observations were made on the melting fraction of the PCM within the PCM panels and the outlet air temperature in the air channels. The enthalpy method was used, which is available in the Ansys package. The present investigation concludes that the developed CFD model adeptly predicts the thermal characteristics of TES during melting and solidifying PCM. The factors influencing the performance of the PAHX are discussed. The results reveal a notable disparity between the time required for melting and that for solidification, with the melting phase exhibiting a significantly shorter duration. Two scenarios have been studied as using PCM–RT21HC in the beginning in the first scenario and followed by PCM–RT25HC and thus will be opposite in the second sce-

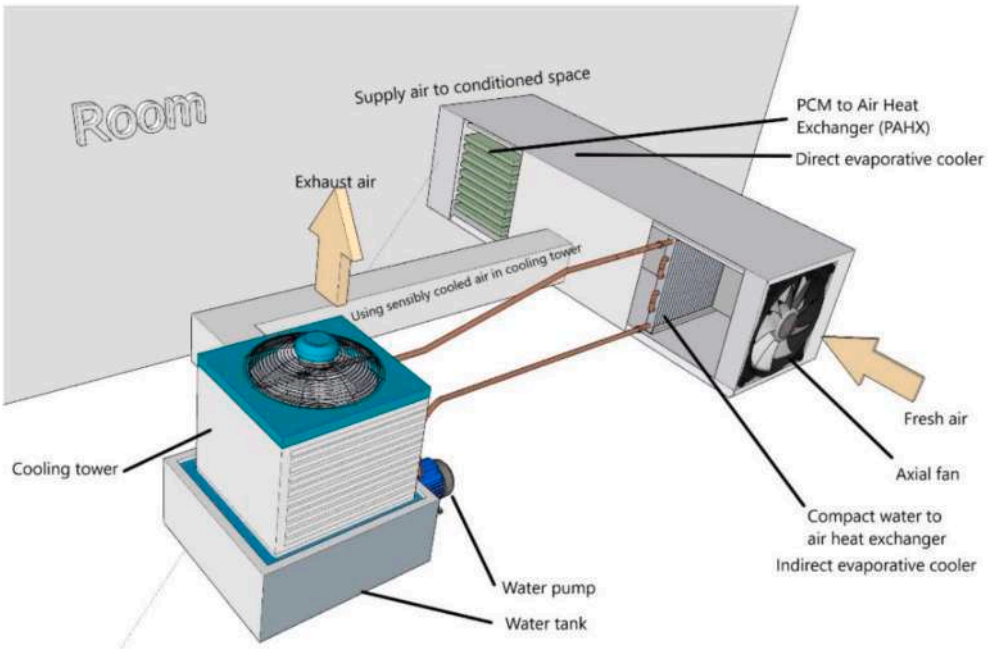

Fig. 7. An illustration of the proposed system [24].

Fig. 8. Experimental rig (photo) [24].

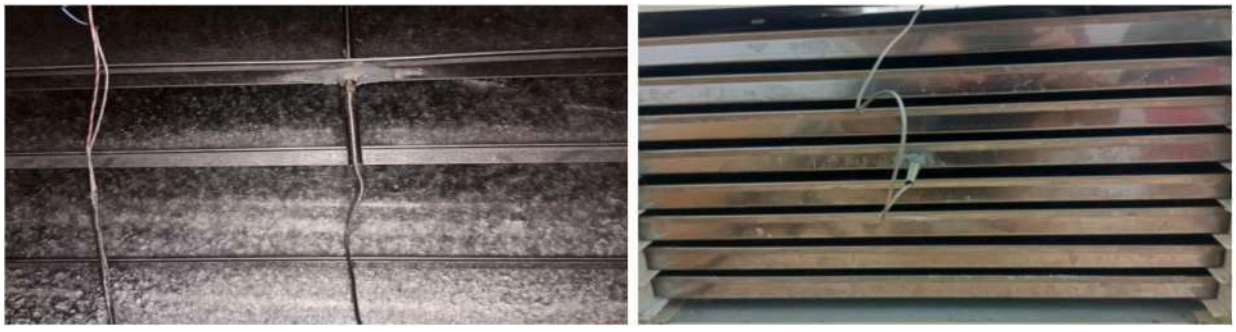

Fig. 9. PCM panels and air channels.

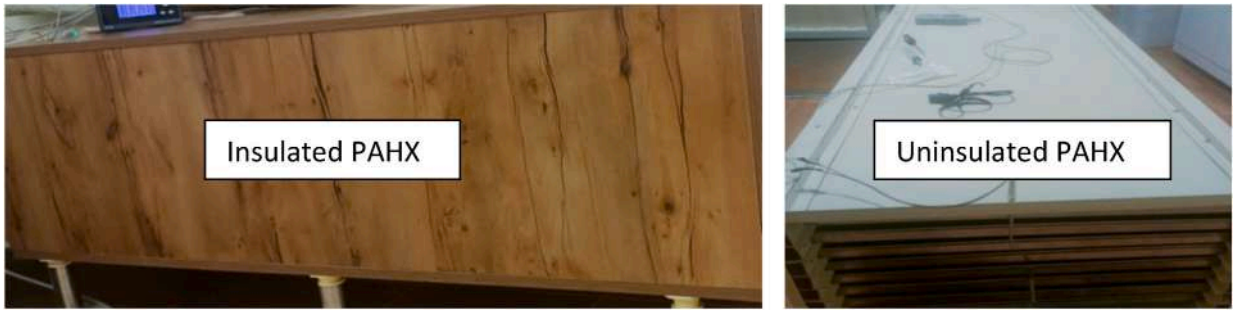

Fig. 10. Photographic view of PAHX.

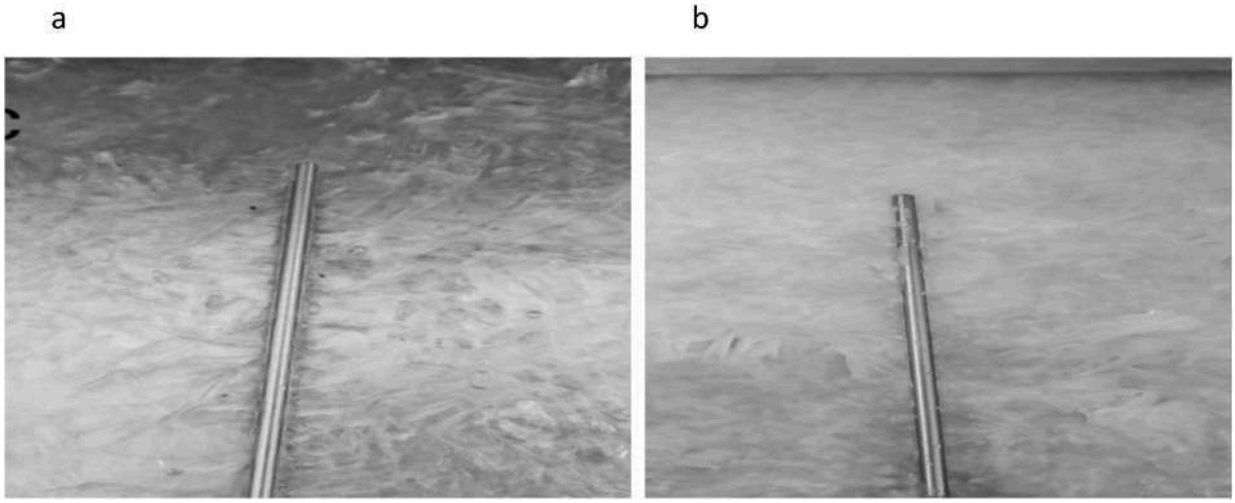

Fig. 11. Solidifying PCM after 6 h (a) PCM-RT21HC partially solidified (b) PCM-RT25HC is completely solidified.

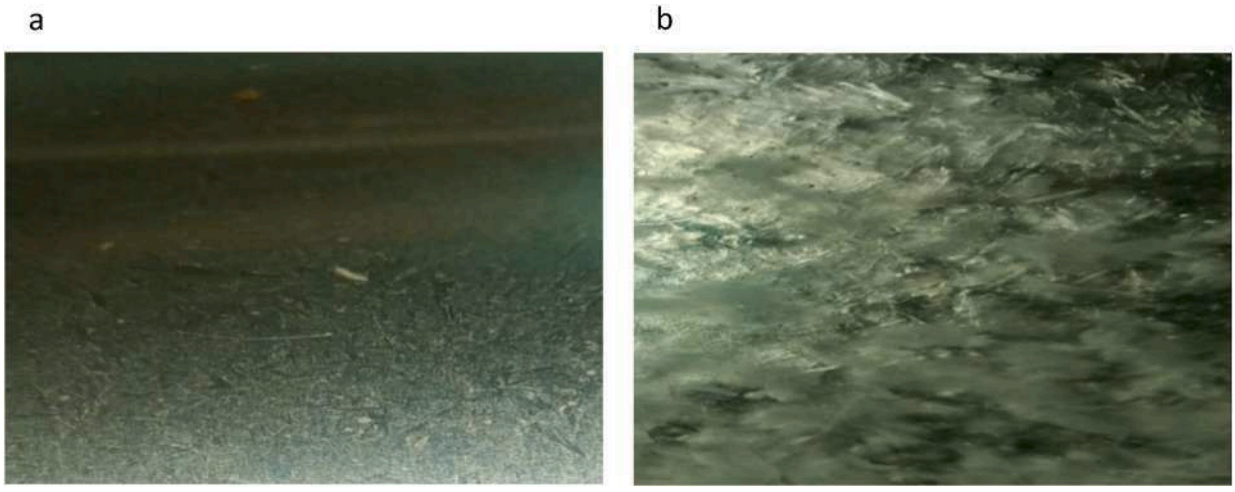

Fig. 12. Melting PCMs after 2 h (a) PCM-RT21HC completely melted (b) PCM-RT25HC partially melted.

nario. The first scenario is recommended for solidification, while the second is more suited for melting. The first scenario is recommended as a solidifying PCM is more challenging than melting. The total time for melting is about (2.5–4 h) while the solidification time exceeds 12 h. The outlet air temperature from the PAHX typically falls within the range of the melting temperatures of both PCMs, indicating that one PCM is in a liquid phase while the other is in a solid phase. Whenever both PCMs melted or solidified, the outlet air temperature of PAHX will exceed those limitations. In the first scenario, the outlet air temperature of the PAHX closely corresponds to PCM–RT25HC, as the PAHX ended with that PCM.

5.1. CFD results

In this section, the CFD results have been represented and discussed. The contour of melting fraction and the outlet air temperature of the PAHX are analyzed during both the melting and solidification processes for both scenarios, as explained in the subsequent sections.

5.1.1. Impact of PCMs sequence with flow direction during solidification

In this section, the solidification time for both scenarios has been studied comparatively. The time is taken for solidifying each PCMs shown individually with a time frame as shown in Fig. (13). Figure (13 a) shows the first scenario, and Fig. (13 b) shows the second scenario. In both cases, the PCM–RT25HC solidified first with a faster solidification rate due to the higher temperature difference between inlet air temperature, which (19 °C) was used for the solidification process compared to PCM–RT21HC. As shown in Fig. (13 b), after 6 h of the solidification process in scenario (2), the PCM–RT25HC is fully solidified compared to scenario (1) which a small portion of the PCM remains in the liquid phase. The reason is that the cooled air is exposed to the RT25 first in the second scenario, and there is a 6 °C temperature difference between the PCM and air. In the second scenario, only PCM-RT25HC solidified after 4 h, whereas PCM-RT21HC was almost liquid. Both PCMs solidified more in the first scenario, with PCM-RT25HC solidifying ultimately

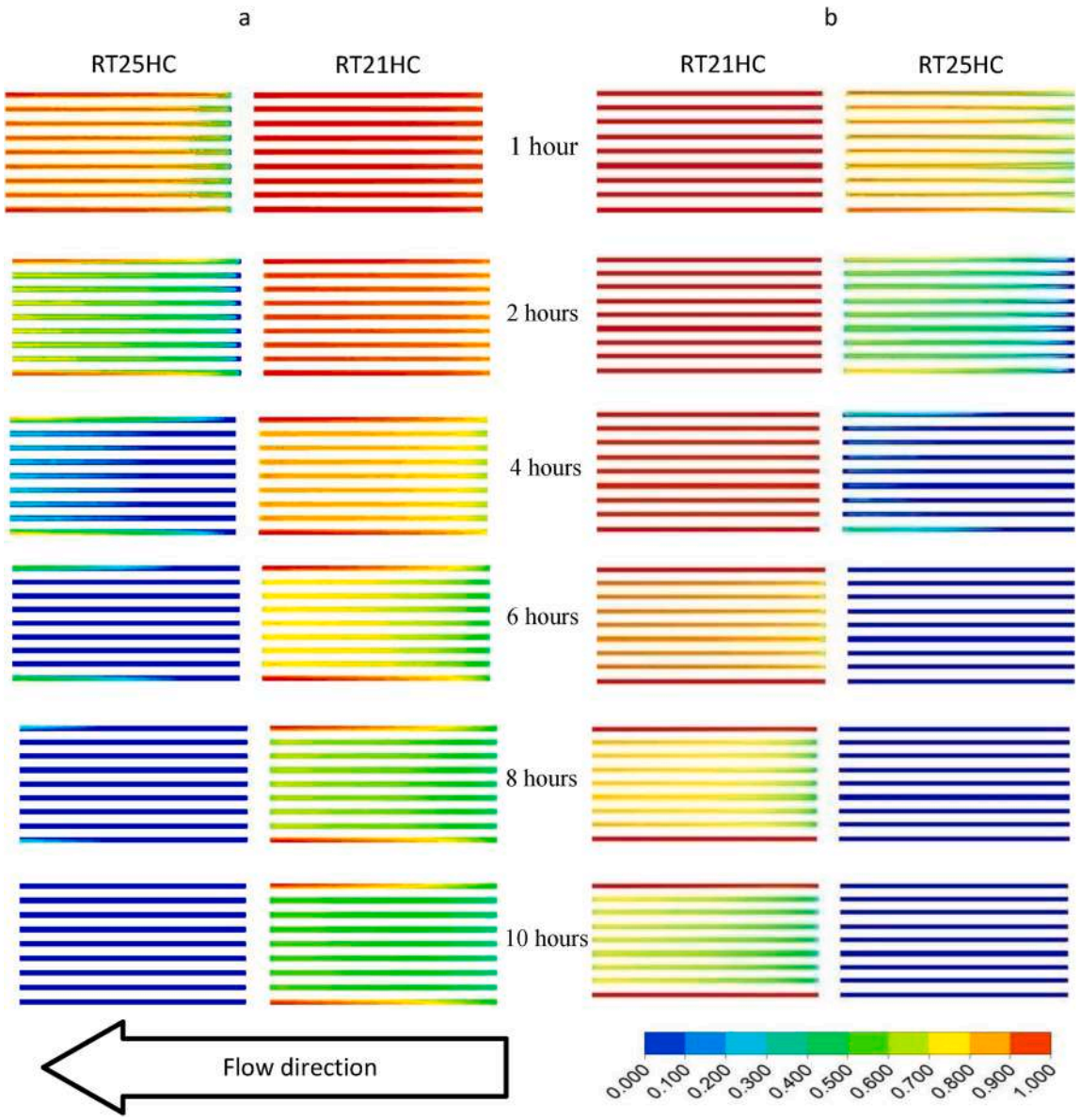

Fig. 13. Liquid fraction for PCM panels during solidification (a) scenario1 & (b) scenario 2.

and PCM-RT21HC partially. The first scenario is typically advised for solidification, and the melting performance of both scenarios will be examined in the next section.

5.1.2. Effect of PCMs sequence with flow direction during melting

This section discusses the performance of both scenarios for the melting process. As shown in Fig. (14), just after 1 h of the melting process, both PCMs RT25HC & RT21HC equally melted in the second scenario. However, for the first scenario, only PCM–RT21HC entirely melted due to a higher temperature difference between PCM and the air (9 °C), while the inlet air temperature used for melting is (30 °C). Another critical point is that after 4 h of melting, both PCMs melted mostly in both scenarios. It is recommended to focus on solidification more than melting since the melting process is more accessible and less time-consuming than the solidification process. The primary reason is that the temperature difference between PCM and the inlet air for melting is higher than solidification, as inlet air for melting and solidification are 30 °C and 19 °C, respectively. The second factor contributing to improved heat transfer during melting is the influence of free convection within PCMs, which predominates when the PCM is in its liquid phase and becomes inactive when the PCM is in its solid phase.

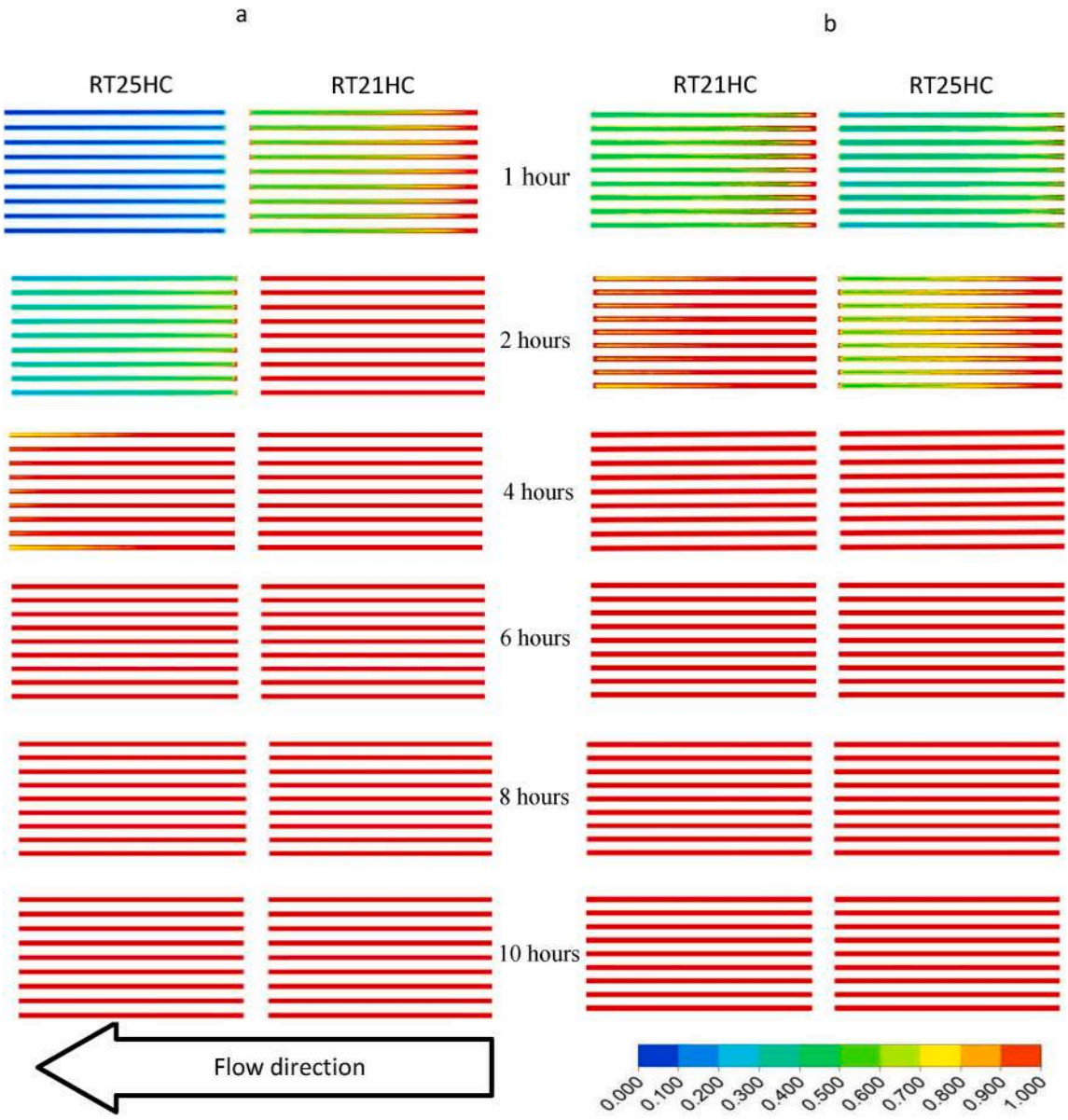

Fig. 14. Liquid fraction for PCM panels during melting (a) scenario 1 & (b) scenario 2.

5.1.3. Melting fraction for scenario (1) during melting and solidification

The melting and solidification processes for scenario (1) involve the observation of the melting fractions in PCMs RT21HC and RT25HC, as well as the melting fraction for the average volume of PCMs. PCM–RT21HC experienced a faster melting process compared to PCM–RT25HC, attributed to the greater temperature differential between the HTF and the melting temperature of the PCM. The PCM–RT21HC is melted in less than 2 h, while PCM–RT25HC needs more than 4 h for entire melting, as shown in Fig. (15). The results are the opposite during solidification, as PCM–RT25HC is solidified much sooner than PCM–RT21HC because of the higher temperature difference between the HTF and PCM's melting temperature. PCM–RT25HC needs 4.5 h for 90 % solidification, but PCM–RT21HC only half is solidified after 12 h. Figures (15 b) show that after 5 h of solidification, 60 % of the total volume of PCM had solidified. Also, after 3 h of melting, 90 % of the total volume of PCM had melted, as shown in Fig. (15 a).

5.1.4. Outlet air temperature in PAHX and the temperature of PCMs in scenario (1) throughout the processes of melting and solidification

The melting and solidification processes for scenario (1) involve the observation of the average temperature within each PCM and the outlet air temperature from the PAHX. Figure (16 a) shows that the average temperature in PCM-RT21HC increased significantly at the beginning of the melting process as an indication of sensibly heated PCM prior to changing its phase because the inlet air is exposed to RT21HC first and then passes through RT25HC. The PCM-RT21HC completely melts within the first 1.5 h, as shown in Fig. (15 a). During melting, the PCM-RT25HC has a lower average temperature at the first 1.5 h, and after that, it has a higher average

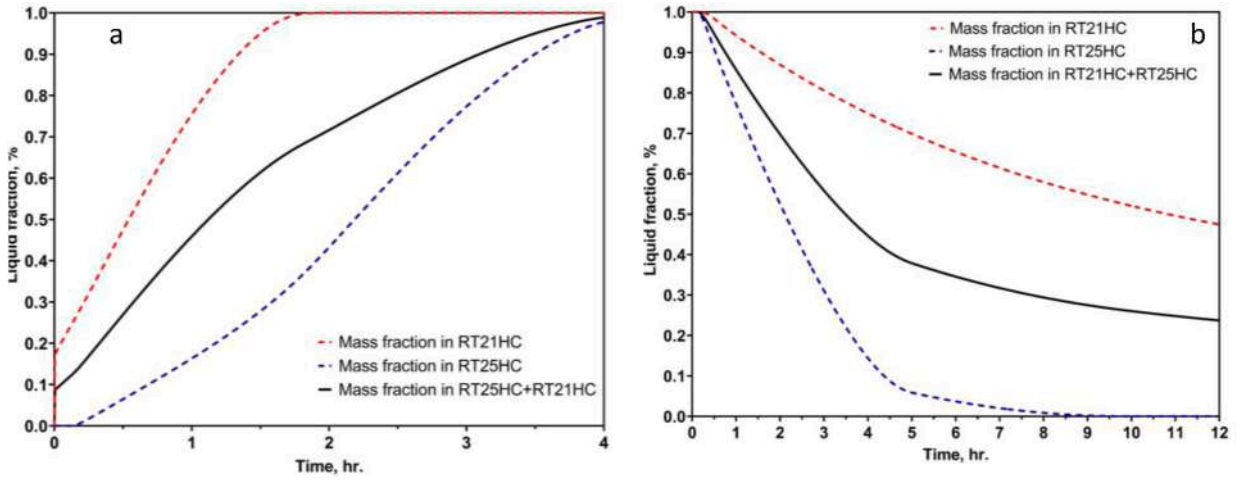

Fig. 15. Total melting and solidification time for PCMs (a) during melting (discharging), (b) during solidification (charging).

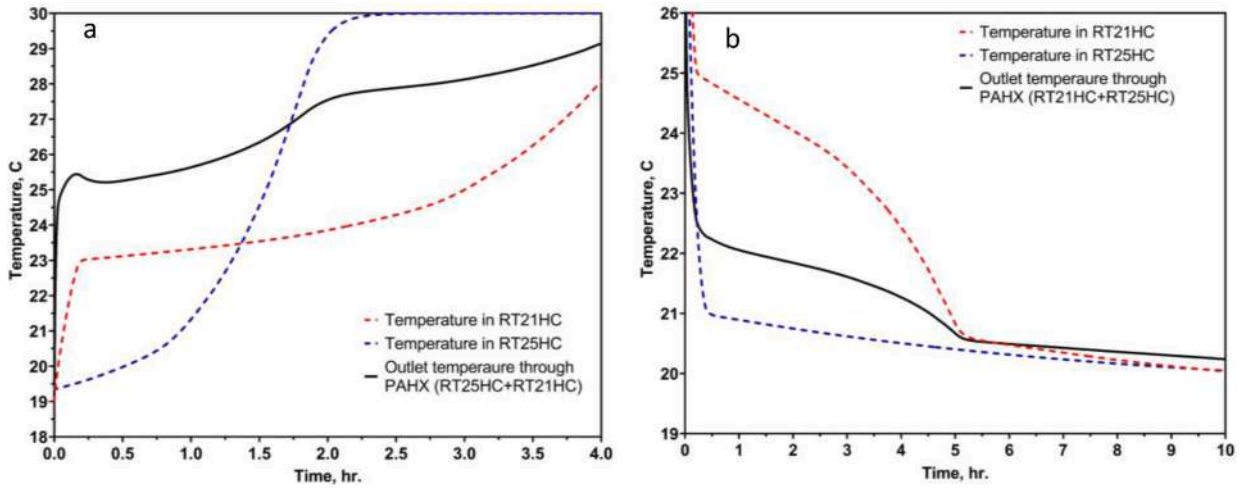

Fig. 16. Outlet air temperature in PAHX and the average temperature in PCMs (a) during melting (discharging), (b) during solidification (charging).

temperature since PCM–RT21HC melted during that time. During melting, the average outlet air temperature from PAHX sharply increased, which indicated sensible heating in PCMs, and after that, the PCMs absorbed latent heat as their temperature increased gradually. The PCM-RT21HC melted more quickly, which melts entirely within the first 1.5 h of melting due to the higher temperature differential between the HTF and the PCM melting temperature. The temperature of PCM-RT25HC at the beginning of the melting is lower than that of RT21HC because RT21HC was the first to come into contact with the warm inlet air. However, the PCM-RT25HC has a higher temperature than the RT21HC after 1.5 h of melting since the PCM-RT21HC has completely melted during that period. During melting, the outlet air temperature is higher than the temperatures of both PCMs as both PCMs release their energy into the air. After 1.75 h of melting, the outlet air temperature will be placed between the temperatures of both PCMs and thus indicating that PCM–RT21HC is entirely melted but PCM–RT25HC is partially melted so that the outlet air temperature will lies between the PCMs temperatures mostly, as shown in Fig. (14) through scenario (1). During solidification, PCM–RT25HC has a higher solidification rate and a lower temperature than PCM–RT21HC for a higher temperature differential between HTF and PCM's melting temperature, as shown in Fig. (15 b). For scenario (1), during solidification, the outlet air temperature of PAHX will be decreased sharply at the beginning of solidification as an indication of releasing sensible heat by PCMs at that time. After that, the PCMs stored latent heat as the outlet air temperature gradually dropped after 0.25 h, as presented in Fig. (16 b).

5.1.5. Melting fraction for scenario (2) during melting and solidification

The liquid fraction in PCMs and average liquid fraction for the average volume of PCMs for the second scenario during melting and solidification has shown in Fig. (17 a & b). During the melting process, PCM–RT21HC will be melted first. The time required for melting PCM–RT21HC and PCM–RT25HC are 2.25 h and 3 h, respectively. The PCM–RT25HC was first solidified during solidification due to the larger temperature difference between HTF and PCM's melting temperature. The time required for entirely solidifying PCM–RT25HC is less than 5 h. However, after 12 h, only 35 % of the PCM– RT21HC solidified and thus showed that the second sce-

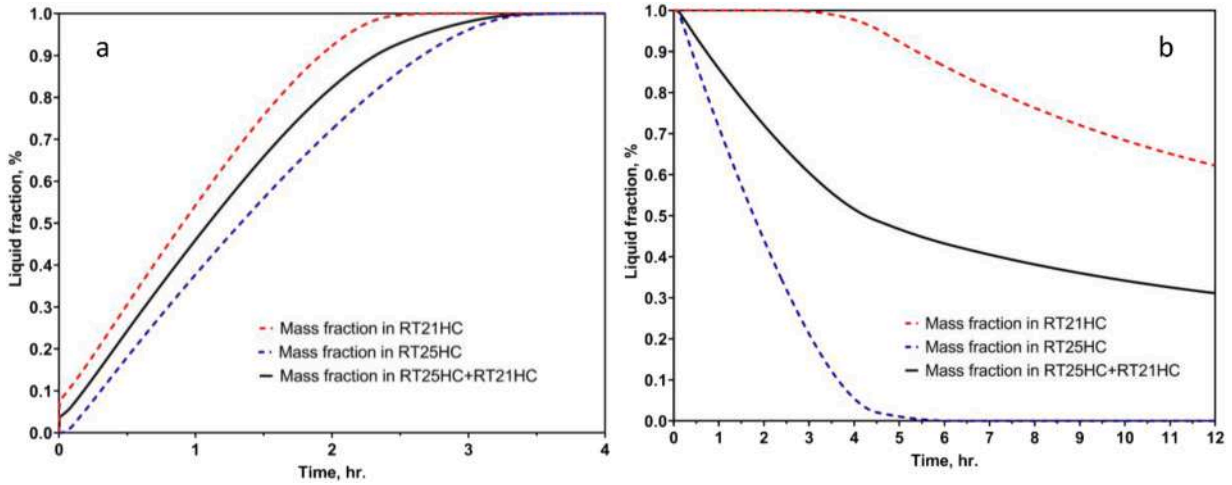

Fig. 17. Illustrates the overall duration of melting and solidification for PCMs, (a) representing the melting (discharging) and (b) representing the solidification (charging).

nario is the worst for solidification, which is disabled to solidifying PCM–RT21HC after 12 h. The first scenario is superior for the solidification process, while the results will be the opposite for melting. The results have clearly shown that the melting time is much shorter than the solidification time due to the boundary conditions and higher temperature differential between PCMs and HTF for melting compared to solidification. The literature confirms that the melting process is less consuming time. Generally, the solidification period lasts three times longer than the melting time. From that point of view, the first scenario is recommended.

5.1.6. Outlet air temperature in PAHX and the temperature of PCMs in scenario (2) throughout the processes of melting and solidification

The outlet air temperature in PHAX and average temperatures in each PCM has shown in Fig. (18 a & b). The average temperature in PCM–RT21HC is raised faster than PCM–RT25HC as the PCM–RT21HC melts faster than PCM–RT25HC due to the larger temperature difference between HTF and PCM's melting temperature. Before 2.25 h of melting, the temperature in PCM–RT21HC is higher than the temperature in PCM–RT25HC, and after that time, its temperature will be lower than PCM–RT25HC and thus indicates that the PCM–RT21HC is entirely melted in that period as shown in Fig. (17 a). During the solidification process, the temperature of PCM–RT25HC dramatically decreases in the first half an hour as the PCM–RT25HC releases sensible heat into the air. After that, its temperature is decreased gradually, as indicated by latent heat and phase transition. PCM–RT21HC has a higher temperature than PCM–RT25HC as it solidified slower than PCM–RT25HC for a lower temperature difference between the air and PCM's melting temperature. The temperature of PCM–RT21HC is lower than PCM – RT25HC after 4.5 h of solidification time as PCM–RT25HC is entirely solidified in that time, as shown in Fig. (17 b). The average outlet air temperature from the PAHX coincides with the temperature of PCM–RT25HC in the first 3.5 h of solidification. After that, it lies between the temperature of both PCMs as a mention to solidify PCM–RT25HC first. During melting, the outlet air temperature is higher than both PCM's temperatures and thus happen due higher

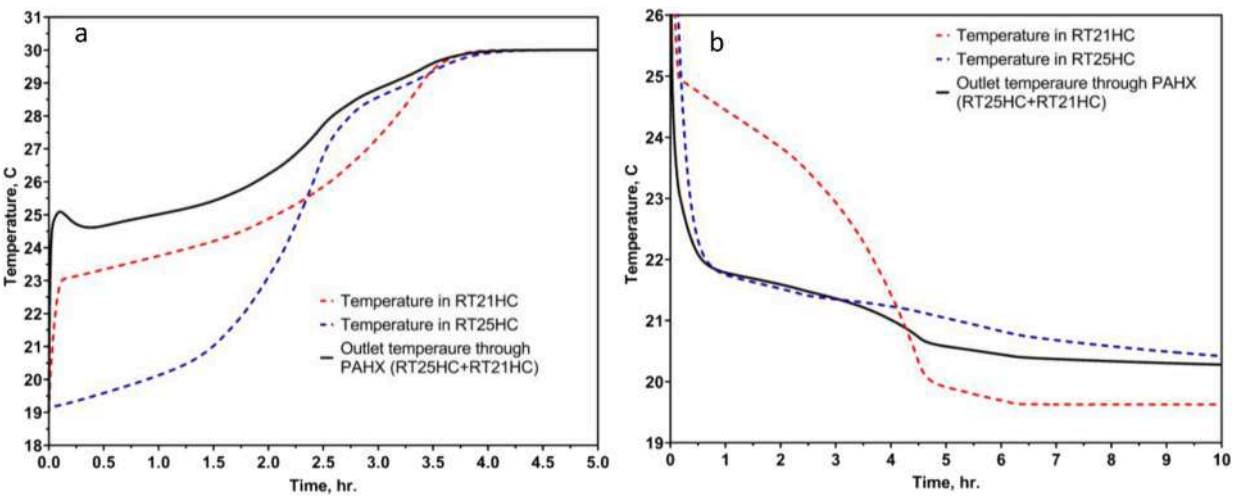

Fig. 18. Outlet air temperature in PAHX and the average temperature in PCMs (a) during melting (discharging), (b) during solidification (charging).

heat transfer rate, firstly from PCM–RT25HC and later PCM–RT21HC, and after 3.5 h of melting, all temperature will have coincided as a confirmation for complete melting of both PCMs as shown in Fig. (17 a).

As shown in Figs. (15 b & 17 b), after 12 h of solidification, the average volume fraction of PCMs in the first and second scenarios is 80 % and 65 %, respectively. Also, after 4 h of the solidification, the average volume fraction of PCMs in the first and second scenarios is 55 % and 45 %, respectively. As shown in Figs. (15 a & 17 a), for the first scenario, the total melting time for 90 % of the volume needs 3 h compared to the second scenario, which is 2.5 h. Moreover, after 2 h of the melting process, 75 % of PCM's volume is melted in the first scenario compared to 85 % for the second scenario for the same period. Overall, the PCMs melt in a reasonable time (3–6 h), but PCMs need a very long time for solidification, which needs more than 12 h, and this is not practical since it is longer than nighttime in summer.

5.2. Experimental results

The experimental results are presented and discussed in this section. As will be elaborated in the following sections, the experimental observations include the average temperature of the PCMs during both the melting and solidification processes, along with the outlet air temperature from the PAHX.

5.2.1. Outlet air temperature from PAHX

In this section, the experimental investigation of the outlet air temperature from the PAHX during the processes of melting and solidifying PCMs is discussed. Indoor thermal comfort is obviously affected by the outlet air temperature from the PAHX, which is directed into the conditioned space. The experimental observation of the outlet air temperature from the PAHX is conducted, and the data is recorded every second in the data logger. This experimental data has been utilized for the validation of the CFD model. The outlet air temperature from the PAHX is observed experimentally during solidifying and melting PCM separately, as detailed in the subsequent sections.

5.2.1.1. a outlet air temperature in PAHX during solidifying. Any PCM that desires to solidify must be cooled with air that is 3–5 °C below its melting point. The sequence of PCMs in the PAHX impacts the melting and solidification rate, so two scenarios have been tested numerically. The first scenario has been constructed in which PCM-RT21HC comes first, followed by PCM-RT25HC. The cooled air with a temperature of 19 °C has been used for solidifying PCMs RT21HC and RT25HC. Cooled air at 19 °C can quickly solidify PCM-RT25HC within 2–4 h, depending on air flow rates, whereas it can solidify PCM-RT21HC partially, as explained through Figs. (13 & 15 a). The average outlet air temperature during solidification from the PAHX is illustrated in Fig. (19). The outlet air temperature decreased in the initial 2 h due to the high solidification rate. However, following that period, the solidification rate reduced, leading to a gradual decrease in the outlet air temperature as the temperature gap between the PCM and HTF narrowed. The maximum deviation between experimental and CFD results is 7 %.

5.2.1.2. b outlet air temperature in PAHX during melting. Hotter air than the PCM's melting point is necessary for any PCM that desires to melt. The first scenario has been constructed in which PCM-RT21HC comes first, followed by PCM-RT25HC. The warmed air with a temperature of 30 °C has been used for melting PCMs RT21HC and RT25HC. The warmed air at 30 °C can melt PCM-RT25HC and PCM-RT21HC, as shown through Figs. (14 & 17 b). The average outlet air temperature from PAHX during the melting process is shown in Fig. (20). The outlet air temperature experienced a rapid increase at the onset of the melting process. Nevertheless, the temperature gradually increased after 0.25 h, meaning the PCMs absorbed much latent heat energy. At the same time, PCM-RT21HC melted, as explained in Fig. (15 a).

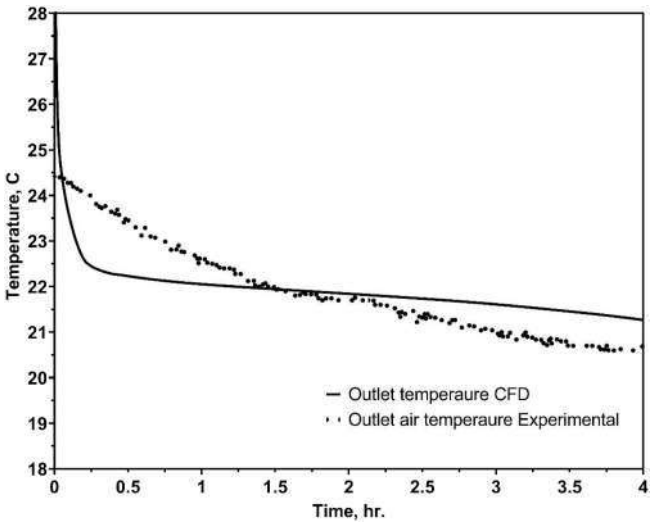

Fig. 19. Outlet air temperature during solidification.

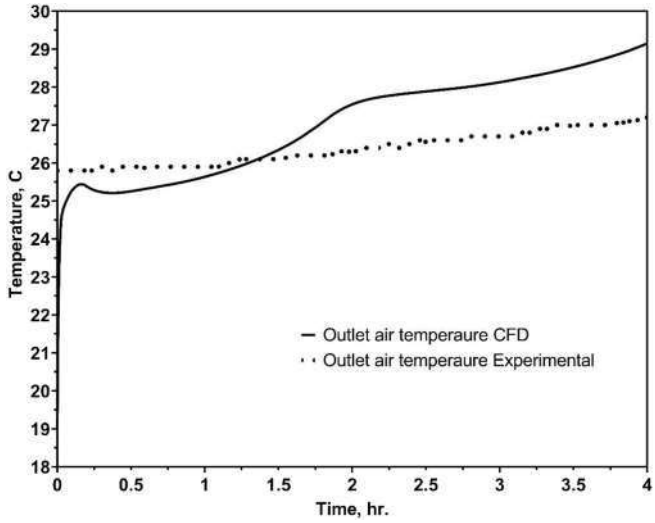

Fig. 20. Outlet air temperature during melting.

5.2.2. *Average temperature in PCMs*

Based on average volume, the average temperature in PCMs is estimated in Ansys CFD and compared with the measured temperature inside PCMs experimentally. Observation of PCM's temperature during the melting and solidification process will help imagine the behavior of the PCMs during melting and solidifying PCMs. In the following sections, recorded measured PCM temperatures are explained and discussed.

5.2.2.1. a Average temperature in PCMs during solidification. Figure (21) show the solidification process in PCMs RT21HC and RT25HC. The experimentally measured data has been used to validate the CFD model. As shown in Fig. (21), the melting temperature of PCM-RT25HC is higher than PCM-RT21HC. The inlet air temperature and mass flow rate in the test are 19 °C and 0.4kg/s, respectively. The solidification rate in PCM-RT25HC is faster than the solidification rate in PCM-RT21HC, and the main reason for that is RT25HC has a higher temperature difference between HTF and the PCM's melting temperature. In the first 2 h, parts of PCM-RT25HC have been solidified, as shown in Fig. (13), and solidifying PCM-RT21HC takes longer. There are some deviations between experimental and CFD results since the multiple PCM model is more complicated due to a heat transfer between PCMs panels. Since the initial temperature for the whole system was set at 30 °C before the solidification process, the temperature of PCM-RT25HC exceeded this value and thus happened due to accumulated heat in PCMs. The average deviation between experimental and CFD results is up to 10 %.

5.2.2.2. b Average temperature in PCMs during melting. Figure (22) show the melting process in PCMs RT21HC and RT25HC. The experimentally measured data has been used to validate the CFD model. As shown in Fig. (22), the transition temperature of PCM-

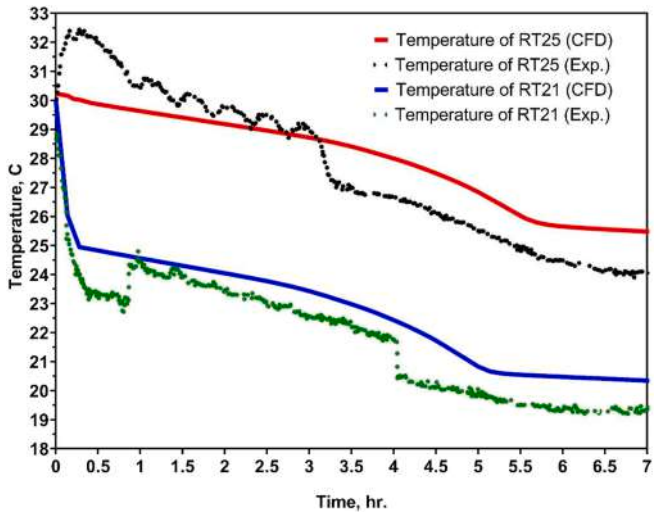

Fig. 21. Average temperature in PCMs during solidification.

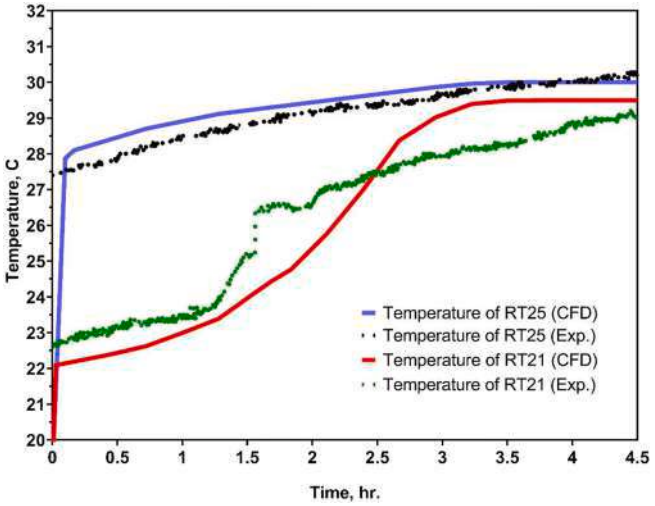

Fig. 22. Average temperature in PCMs during melting.

RT25HC is higher than PCM-RT21HC. The inlet air temperature and mass flow rate in the test are 30 °C and 0.4kg/s, respectively. The melting rate in PCM-RT21HC is faster than in PCM-RT25HC, and the main reason is that RT21HC has a higher temperature difference between HTF and the PCM's melting temperature. In the first 2 h, the PCM-RT21HC has been melted entirely, as shown in Fig. (13), and melting PCM-RT25HC takes longer. The temperature in PCM-RT21HC at the beginning sharply increased due to sensible heat release from the PCM to HTF. The temperature of the PCM-RT21HC has been nearly constant after 3 h of melting, which means the PCM-RT21HC is entirely melted. The melting process in PCM-RT25HC needs more than 4 h, as shown in Fig. (14). There are some deviations between experimental and CFD results since the multiple PCM model is complicated. The initial temperature for the whole system was set at 19 °C before beginning the melting process. The average deviation between experimental and CFD results is up to 12 %.

6. Conclusions

The PAHX was investigated numerically and experimentally in this study to melt and solidify PCMs RT25HC and RT21HC. The CFD model 2D has been built for PAHX from ANSYS (Fluent 19.2). The utilization of the CFD model for numerical testing of various PCMs with distinct melting temperatures is attributed to the low thermal conductivity of both air and PCMs. Based on the CFD results, the heat transfer between HTF and PCMs can be enhanced by incorporating multiple PCMs. The arrangement of PCM sequences in a series has an impact on the melting and solidification processes of PCMs. Two scenarios have been designed and tested in the CFD model. In the first scenario, PCM-RT21HC is utilized first, succeeded by PCM-RT25HC, whereas the order of usage is reversed in the second scenario. The first scenario is recommended for achieving a quicker solidification rate, but the second scenario demonstrates superior performance during the melting. The solidification process necessitates a significantly longer duration when compared to the melting process, so the first scenario has been adapted and experimentally investigated. The maximum deviations between CFD and experimental exist as 12 % in PCM's temperatures during melting and solidification and thus happen for the complexity of using multiple PCMs in PAHX. The PAHX has been designed with the optimum results of the CFD model. The key factor affecting the rates of melting and solidification in PCMs is the temperature difference between the inlet HTF and the melting temperature of the PCM. The experimental data has been used to validate CFD models. Employing PCM-RT25HC and PCM-RT21HC to maintain the outlet air temperature from the PAHX within a comfortable range of 21–25 °C, the experimental findings indicated that the outlet air temperature from the PAHX is difficult to overpass that temperature limit. The key findings of this study are provided below.

- PCM-RT25HC underwent rapid solidification in both scenarios, completing the process in 4 h, whereas PCM-RT21HC took more than 12 h to fully solidify.
- PCM-RT21HC exhibited a faster melting rate than PCM-RT25HC, attributed to a higher temperature difference between HTF and the PCM's melting temperature. However, both PCMs melted completely within 4 h.
- The time required for both melting and solidification decreases with a reduction in PCM panel thickness, a decrease in air channel height, an increase in PCM panel length, and higher flow rates. The crucial factor influencing variations in melting and solidification time is the temperature difference between HTF and the PCM's melting temperature.
- A greater influence is observed from an increased temperature differential between HTF and PCM melting compared to higher HTF flow rates.
- Experimentally, the use of multiple PCMs in series has been employed to improve the heat transfer rate between air and PCMs. The findings demonstrated a decrease in both solidification and melting times when multiple PCMs were utilized instead of a single PCM.

- The heat transfer rate between HTF and PCMs is affected by the sequence of PCM utilization in a series, prompting the examination of two scenarios. In the first scenario, PCM-RT21HC is applied first, followed by PCM-RT25HC, while in the second scenario, the order is reversed. The results indicate that the first scenario contributes to a reduction in solidification time, while the second scenario can decrease melting time.
- The system can provide free cooling and ventilation for the conditioned zone despite the system's prolonged thermal comfort time in the building. The supply air temperature to the conditioned space is mostly between 21 and 25 °C because the PCM-RT21HC must release a lot of heat energy to allow the outlet air temperature to be lower than PCM's melting temperature. Also, to overcome 25 °C, the PCM-RT25HC must absorb much heat energy before increasing the outlet air temperature.

CRediT authorship contribution statement

Bashir Eskander Kareem: Writing – original draft, Validation, Software, Resources, Methodology, Investigation, Data curation, Conceptualization. **Ahmed Mohammed Adham:** Writing – review & editing, Supervision, Resources, Investigation, Conceptualization. **Banipal Nanno Yaqob:** Writing – review & editing, Visualization, Validation, Supervision, Investigation, Conceptualization.

Declaration of competing interest

The authors declare that they have no known competing financial interests or personal relationships that could have appeared to influence the work reported in this paper.

Data availability

Data will be made available on request.

References

[1] Key World Energy Statistics, 2021, OECD, 2021, https://doi.org/10.1787/2ef8cebc-en.
[2] B.E. Kareem, A.M. Adham, B.N. Yaqob, Performance enhancement of a ventilation system in hot and dry climate using air-PCM heat exchanger, International Journal of Heat and Technology 40 (2022) 773–780, https://doi.org/10.18280/ijht.400316.
[3] J. Ding, H. Zhang, D. Leng, H. Xu, C. Tian, Z. Zhai, Experimental investigation and application analysis on an integrated system of free cooling and heat recovery for data centers, Int. J. Refrig. 136 (2022) 142–151, https://doi.org/10.1016/J.IJREFRIG.2022.01.003.
[4] H.H. Jo, Y. Kang, S. Yang, Y.U. Kim, B.Y. Yun, J.D. Chang, S. Kim, Application and evaluation of phase change materials for improving photovoltaic power generation efficiency and roof overheating reduction, Renew. Energy 195 (2022) 1412–1425, https://doi.org/10.1016/J.RENENE.2022.06.119.
[5] M. Teggar, A. Laouer, A. Benhorma, H. Goudjil, M. Arıcı, K.A. Ismail, S. Mekhilef, E.H. Mezaache, T. Tahouri, Perspective role of phase change materials for energy efficiency in Algeria, Renew. Energy 217 (2023) 119203, https://doi.org/10.1016/J.RENENE.2023.119203.
[6] P. Hlanze, Z. Jiang, J. Cai, B. Shen, Model-based predictive control of multi-stage air-source heat pumps integrated with phase change material-embedded ceilings, Appl. Energy 336 (2023) 120796, https://doi.org/10.1016/J.APENERGY.2023.120796.
[7] A. Ahmad, S.A. Memon, A novel method to evaluate phase change materials' impact on buildings' energy, economic, and environmental performance via controlled natural ventilation, Appl. Energy 353 (2024) 122033, https://doi.org/10.1016/J.APENERGY.2023.122033.
[8] J. Yu, C. Qian, Q. Yang, T. Xu, J. Zhao, X. Xu, The energy saving potential of a new ventilation roof with stabilized phase change material in hot summer region, Renew. Energy 212 (2023) 111–127, https://doi.org/10.1016/J.RENENE.2023.05.012.
[9] N. Bianco, A. Fragnito, M. Iasiello, G.M. Mauro, A CFD multi-objective optimization framework to design a wall-type heat recovery and ventilation unit with phase change material, Appl. Energy 347 (2023) 121368, https://doi.org/10.1016/J.APENERGY.2023.121368.
[10] E.M.S. El-Said, A.H. Elsheikh, H.R. El-Tahan, Effect of curved segmental baffle on a shell and tube heat exchanger thermohydraulic performance: numerical investigation, Int. J. Therm. Sci. 165 (2021), https://doi.org/10.1016/j.ijthermalsci.2021.106922.
[11] E.M.S. El-Said, M. Abd Elaziz, A.H. Elsheikh, Machine learning algorithms for improving the prediction of air injection effect on the thermohydraulic performance of shell and tube heat exchanger, Appl. Therm. Eng. 185 (2021), https://doi.org/10.1016/j.applthermaleng.2020.116471.
[12] F. He, R. Bo, C. Hu, X. Meng, W. Gao, Employing spiral fins to improve the thermal performance of phase-change materials in shell-tube latent heat storage units, Renew. Energy 203 (2023) 518–528, https://doi.org/10.1016/J.RENENE.2022.12.091.
[13] F. Bre, R. Lamberts, S. Flores-Larsen, E.A.B. Koenders, Multi-objective optimization of latent energy storage in buildings by using phase change materials with different melting temperatures, Appl. Energy 336 (2023) 120806, https://doi.org/10.1016/J.APENERGY.2023.120806.
[14] K. Zhao, J. Wang, H. Xie, Z. Guo, Microencapsulated phase change n-Octadecane with high heat storage for application in building energy conservation, Appl. Energy 329 (2023) 120284, https://doi.org/10.1016/J.APENERGY.2022.120284.
[15] A. Arshad, H.M. Ali, W.M. Yan, A.K. Hussein, M. Ahmadlouydarab, An experimental study of enhanced heat sinks for thermal management using n-eicosane as phase change material, Appl. Therm. Eng. 132 (2018) 52–66, https://doi.org/10.1016/j.applthermaleng.2017.12.066.
[16] F. Khlissa, M. Mhadhbi, W. Aich, A.K. Hussein, M. Alhadri, F. Selimefendigil, H.F. Öztop, L. Kolsi, Recent advances in nanoencapsulated and nano-enhanced phase-change materials for thermal energy storage: a review, Processes 11 (2023), https://doi.org/10.3390/pr11113219.
[17] L. Kolsi, A.K. Hussein, W. Hassen, L. Ben Said, B. Ayadi, W. Rajhi, T. Labidi, A. Shawabkeh, K. Ramesh, Numerical study of a phase change material energy storage tank working with carbon nanotube–water nanofluid under ha'il city climatic conditions, Mathematics 11 (2023), https://doi.org/10.3390/math11041057.
[18] F.L. Rashid, M.A. Al-Obaidi, N.S. Dhaidan, A.K. Hussein, B. Ali, M.B. Ben Hamida, O. Younis, Bio-based phase change materials for thermal energy storage and release: a review, J. Energy Storage 73 (2023) 109219, https://doi.org/10.1016/J.EST.2023.109219.
[19] E. Banoqitah, R. Sathyamurthy, E.B. Moustafa, M. Fujii, P. Sudalaimuthu, F. Djouider, A.H. Elsheikh, Enhancement and prediction of a stepped solar still productivity integrated with paraffin wax enriched with nano-additives, Case Stud. Therm. Eng. 49 (2023), https://doi.org/10.1016/j.csite.2023.103215.
[20] A. Lazaro, P. Dolado, J.M. Marín, B. Zalba, PCM-air heat exchangers for free-cooling applications in buildings: experimental results of two real-scale prototypes, Energy Convers. Manag. 50 (2009) 439–443, https://doi.org/10.1016/j.enconman.2008.11.002.
[21] U. Stritih, An experimental study of enhanced heat transfer in rectangular PCM thermal storage, Int. J. Heat Mass Tran. 47 (2004) 2841–2847, https://doi.org/10.1016/j.ijheatmasstransfer.2004.02.001.
[22] P. Dolado, A. Lazaro, J.M. Marin, B. Zalba, Characterization of melting and solidification in a real scale PCM-air heat exchanger: numerical model and experimental validation, Energy Convers. Manag. 52 (2011) 1890–1907, https://doi.org/10.1016/j.enconman.2010.11.017.
[23] B.E. Kareem, A.M. Adham, B.N. Yaqob, Design and optimization of air to PCM heat exchanger using CFD, Arabian J. Sci. Eng. 48 (2023) 12609–12623, https://doi.org/10.1007/s13369-022-07360-w.
[24] B.E. Kareem, A.M. Adham, B.N. Yaqob, Experimental analysis of air-multiple pcm heat exchanger in evaporative cooling systems for supply air temperature stabilization, J. Build. Eng. 82 (2024), https://doi.org/10.1016/j.jobe.2023.108269.